EMERGING ADVANCES IN INTEGRATED TECHNOLOGY
e-ISSN: 2773-5540

EmAIT

Vol. 6 No. 2 (2025) 45-55
https://publisher.uthm.edu.my/ojs/index.php/emait

Simulation Study of n-type Double-Gate Nano-MOSFET with Arbitrary Wafer Orientations and Any Channel Materials

Ooi Chek Yee[1]*, Wong Pei Voon[1]

[1] *Faculty of Information and Communication Technology,*
Universiti Tunku Abdul Rahman, Jalan Universiti, Bandar Barat, 31900 Kampar, Perak, MALAYSIA

*Corresponding Author: ooicy@utar.edu.my
DOI: https://doi.org/10.30880/emait.2025.06.02.005

Article Info

Received: 22 January 2025
Accepted: 22 April 2025
Available online: 31 December 2025

Keywords

Wafer orientation, channel material, Nano-MOSFET, effective mass, quantum effects

Abstract

In this paper, the technique for quantum mechanically simulating a double-gate (DG) nano-MOSFET with arbitrarily oriented wafer directions and various channel materials is presented. The problem with arbitrarily oriented wafer directions and any channel materials is that the misalignment of principal axes of conduction bands ellipsoids and devices axes causes the matrix and so effective mass equation (EME) become cumbersome to solve. This drawback is overcome by transforming the main axes of the conduction band ellipsoids of the nano-MOSFET to align properly with the device axes, that are transport, confinement and width directions. This transformation technique is discussed theoretically, generally and then simulated specifically for a 10 nm n-type DG nano-MOSFET designed using Silicon (Si) wafer orientation of (100) direction. Two current-voltage (I-V) equations are derived and the calculated on-state current value, $\boldsymbol{I_{on}}$ are compared with theoretically simulated data 2.500x10^3 µA/µm. The first and second current model produce $\boldsymbol{I_{on}}$ of 2.182x10^3 µA/µm and 2.548x10^3 µA/µm, respectively. The second model is more accurate since it treats the electron flow as ballistic. This transformation technique enables device engineers to use any device simulator with EME model to study the carriers transport properties of MOSFET with any channel materials (Si, Ge and GaAs) and arbitrary wafer orientations ((100), (110) and (111)). This paper focuses specifically on Si with (100) wafer.

---

1. Introduction

Nowadays, the most common semiconductor materials that can be used in fabrication of semiconductor nanodevices include Si, Ge and GaAs [1-4]. The orientations of the wafers made from these materials can affect the electronic properties of the nanotransistors thus fabricated. The study of arbitrary wafer orientations of these materials is difficult to carry out by device simulators because the conduction band energy ellipsoids are not nicely aligned with the transistors' device axes [5-6]. This problem incurred the solution of the device simulator to become non-trivial [7]. To eliminate this hindrance, device designers can apply a technique which transforms the arbitrarily oriented energy ellipsoids to align neatly with nanotransistors dimensional axes in thickness, channel and width directions before performing simulation [8-9].

Silicon (100) wafer is chosen as the specific study in this paper due to its mature process technology compares to other materials. Efficient Si wafer orientation can increase the process yield. It also can affect the dissipation of heat and the quantity of ion implantation [10]. The (100) orientation direction is selected rather than (110) and (111) because (100) oriented Si wafers are more suitable for fabricating modern logical integrated circuits, such as microprocessors, because of the following reasons [11-14]; (i.) smooth (100) surface can accommodate greater transistors density, (ii.) high quality of thermal oxide growth enabling superior insulator dielectrics, and (iii.) better ion implantation through oxide layer.

2. Device Design

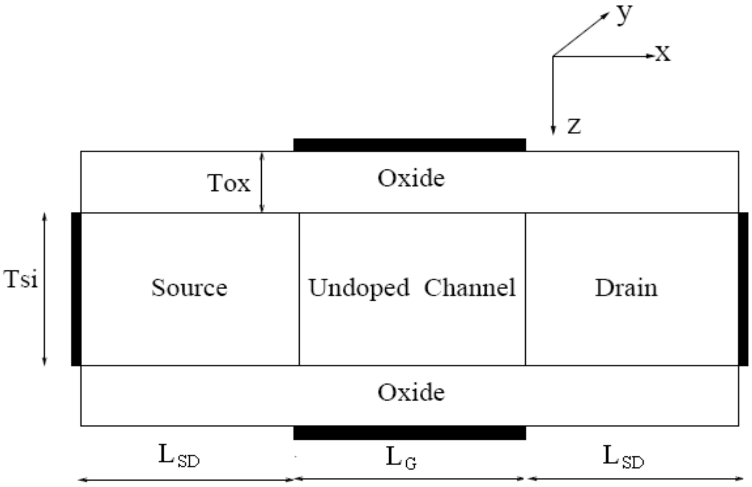

Fig. 1 *Double-gate nano-MOSFET device structure diagram. The wavevectors along transport, width and thickness directions are* k_1 *(or* k_x*),* k_2 *(or* k_y*) and* k_3 *(or* k_z*), respectively*

Table 1 *Double-gate nano-MOSFET device structural simulation parameters*

Parameters	Value
Drain-to-Source Voltage Bias (V_{DS})	0.60 V
Gate-to-Source Voltage Bias (V_{GS})	0.60 V
Threshold Voltage (V_T)	0.20 V
Simulation Temperature	300 K
Source/Drain Doping Concentration (N_D)	1x10^{20} cm^{-3}
Body Doping Concentration	intrinsic
Silicon Channel Thickness (T_{Si})	1.5 nm
Source/Drain Overlap	0 nm
Source Length/Drain Length (L_{SD})	7.5 nm
Channel Length (L)	10 nm
Top/Bottom Oxide Insulator Thickness (T_{OX})	1.5 nm
Top/Bottom Insulator Relative Dielectric Constant (SiO_2)	3.9
Longitudinal Relative Electron Mass Ratio (m_l)	0.98
Transverse Relative Electron Mass Ratio (m_t)	0.19
Channel Body Relative Dielectric Constant (Si)	11.7
Top/Bottom Gate Contact Work Function	4.188 eV
Silicon Conduction Band Valleys	unprimed
Number of Subbands	1

Figure 1 shows the generalized symmetric structure of DG nano-MOSFET used in this study [15-16]. In this investigation, the specific channel material used is Si because of its mature and advanced fabrication technology and abundance on this planet. Table 1 indicates the simulation parameter used in nanoMOS which is a free on-line device simulator [17-18]. The unprimed subbands of conduction band valleys are choosen because of its lower bound-state energies due to the heavier longitudinal mass. Meanwhile, total number of subbands is set to 1.

Wafer direction (100) is selected for this study rather than (110) and (111) directions because of the perfect alignment of conduction band ellipsoids along device coordinate system and thereby tremendously reduce simulation computational burden. In reality, crystalline plane with Miller index (100) is parallel with x coordinate axis, (010) crystalline plane is parallel to y axis and (001) plane is parallel with z axis. Thus, (100) direction is the same as (010) and also (001). Si wafers with (100) orientation are used widely to fabricate CMOS integrated circuits (ICs) [19,20]. (110) wafer orientation silicon wafers are mainly used in situation with higher requirement of hole mobility. Meanwhile, (111) wafer orientation silicon wafers are commonly used in fabricating bipolar devices where better hole and electron movement control is needed.

As electron devices scaled down to nanometer regime, classical conventional transport model which is drift diffusion equation is unable to precisely described the carrier properties of nanotransistors due to existence of quantum confinement. Instead, quantum model must be adopted to examine the transport properties of nanodevices. Table 2 below summarized these approaches.

Table 2 *Comparison between quantum mechanical simulation and classical transport simulation*

Simulation Transport Model	Quantum Mechanical	Drift Diffusion
Treatment of Carriers	Wave nature	Particle nature
Device Dimensional Structure	Nanometer regime	Micrometer (bulk)
Simulation Approach	Non-Equlibrium Green's Function (NEGF)	Boltzmann Transport Equation (BTZ)
Result Accuracy at Nanoscale Devices	High	Low

3. Theoretical Reviews of Any Channel Materials in Nano-MOSFET

3.1 Conduction Band in Semiconductor

The constant energy band surface in the direct band gap semiconductor material, such as GaAs, is spherical in shape and can be expressed as

$$E = \frac{\hbar^2 k^2}{2m_{eff}} \tag{1}$$

where m_{eff} is the isotropic effective mass. Meanwhile, at indirect semiconductor materials, like Si, the conduction energy band surfaces are ellipsoidal in shape revolving around Δ and Λ axes. These bands can be described by two effective masses, that is longitudinal mass, m_l, and transverse mass, m_t. There are three orthogonal coordinate systems; namely, device coordinate system (DCS), crystal coordinate system (CCS) and ellipsoid coordinate system (ECS), which are used to formulate and simplify the EME for quantum transport simulation of nano-MOSFETs. The DCS depends on wafer orientation and fabrication process choice whereas the ECS relies on the choice of channel material. The constant energy ellipsoid is described by

$$E = \frac{\hbar^2 k_{||}^2}{2m_l} + \frac{\hbar^2 (k_{\perp 1}^2 + k_{\perp 2}^2)}{2m_t} \tag{2}$$

where $k_{||}$, $k_{\perp 1}$ and $k_{\perp 2}$ are wavevectors in ECS. According to [21], the inverse effective mass tensor (EMT) is a 3x3 diagonal matrix with m_l^{-1}, m_t^{-1}, and m_t^{-1} along the diagonal. $\mathfrak{R}_{E \leftarrow C}$ is a 3x3 rotation matrix that transform arbitrary wavevectors in CCS to ECS components. A similar rotation matrix $\mathfrak{R}_{C \leftarrow D}$ transforms wavevectors in DCS to CCS components. Therefore, for a given conduction band ellipsoid and channel material, the overall rotation matrix from DCS to ECS are defined as

$$\mathfrak{R}_{E \leftarrow D} = \mathfrak{R}_{E \leftarrow C} \mathfrak{R}_{C \leftarrow D} \tag{3}$$

Let $a_{ij} = [\mathfrak{R}_{E \leftarrow D}]_{ij}$, the inverse EMT is a full 3x3 symmetric matrix which can be calculated by

$$\frac{1}{m_{ij}} = \frac{a_{1i}a_{1j}}{m_l} + \frac{a_{2i}a_{2j} + a_{3i}a_{3j}}{m_t} \tag{4}$$

Since $m_{ij} = m_{ji}$, Equation (2) can be rewritten as

$$E(k_1,k_2,k_3)=\sum_{i=1}^{3}\frac{\hbar^2k_i^2}{2m_{ii}}+2\sum_{i=1}^{3}\sum_{i<j\le 3}\frac{\hbar^2k_ik_j}{2m_{ij}} \tag{5}$$

When comparing with Equation (1), the constant energy ellipsoidal surface stated in Equation (5) has additional kinetic energy cross terms k_ik_j which causes the EME to become non-trivial during computational simulation. For the specific Si (100) wafer studied in this work, the EMT matrix is diagonal and so the cross terms in Equation (5) disappeared. Hence, the simulation can be performed nicely since the EME can be calculated without troublesome. On the other hand, the simulation of arbitrarily oriented wafer and any channel materials, such as Ge (100) wafer as well as Si (111) or (110) wafers, are unnecessarily complicated because the EMT in DCS are full 3x3 matrix. However, under certain simplifying conditions, as will be explained in next subsections, this limitation of EME is eliminated.

3.2 The Universal Effective Mass Equation (EME)

Applying the labels for DCS axes in Figure 1, Equation (5) becomes

$$E(k_x,k_y,k_z)=\frac{\hbar^2k_x^2}{2m_{11}}+\frac{\hbar^2k_y^2}{2m_{22}}+\frac{\hbar^2k_z^2}{2m_{33}}+\frac{\hbar^2k_xk_y}{m_{12}}+\frac{\hbar^2k_yk_z}{m_{23}}+\frac{\hbar^2k_zk_x}{m_{31}} \tag{6}$$

After replacing $k_x \rightarrow -i\partial/\partial x$ and $k_z \rightarrow -i\partial/\partial z$, the corresponding 2D Schrodinger effective mass equation is expressed as

$$\begin{aligned}\left[-\frac{\hbar^2}{2m_{11}}\frac{\partial^2}{\partial x^2}-i\frac{\hbar^2k_y}{2m_{12}}\frac{\partial}{\partial x}+\frac{\hbar^2k_y^2}{2m_{22}}+\left\{-\frac{\hbar^2}{2m_{33}}\frac{\partial^2}{\partial z^2}-i\hbar^2\left(\frac{k_y}{m_{23}}-i\frac{1}{m_{31}}\frac{\partial}{\partial x}\right)\frac{\partial}{\partial z}+W(x,z)\right\}\right]\Psi_{k_y}(x,z)\\ =E\Psi_{k_y}(x,z)\end{aligned} \tag{7}$$

where $W(x,z)$, which is independent of y because the potential is unvarying along width direction, is the potential energy. In order to solve the problem mentioned in this paper, mode space formalism is used when discussing, (i.) quantum confinement problem, and (ii.) transport problem.

3.2.1 Quantum Confinement Problem

The Hamiltonian related to confinement potential is diagonalized by confinement modes. From Equation (7), quantum confinement problem at any point of x is separated into different terms. After performing canonical transformation to confinement problem, Equation (7) can be rewritten as

$$[H_z+W(x,z)]e^{-i\left(\frac{m_{33}}{m_{23}}k_y-i\frac{m_{33}}{m_{31}}\frac{\partial}{\partial x}\right)z}\phi_i(x,z)=\left\{\epsilon_i(x)-\epsilon\left(-i\frac{\partial}{\partial x},k_y\right)\right\}e^{-i\left(\frac{m_{33}}{m_{23}}k_y-i\frac{m_{33}}{m_{31}}\frac{\partial}{\partial x}\right)z}\phi_i(x,z) \tag{8}$$

where the *i*-th subband energy at x is $\epsilon_i(x)$, ϕ_i's is the modes and kinetic energy is given by

$$\epsilon\left(-i\frac{\partial}{\partial x},k_y\right)=\frac{\hbar^2}{2}\left(-\frac{m_{33}}{m_{31}^2}\frac{\partial^2}{\partial x^2}+\frac{m_{33}}{m_{32}^2}k_y^2-2i\frac{m_{33}}{m_{31}m_{23}}k_y\frac{\partial}{\partial x}\right) \tag{9}$$

In addition, the confinement Hamiltonian is given by

$$H_z=-\frac{\hbar^2}{2m_{33}}\frac{\partial^2}{\partial z^2}-i\hbar^2\left(\frac{k_y}{m_{23}}-i\frac{1}{m_{31}}\frac{\partial}{\partial x}\right)\frac{\partial}{\partial z} \tag{10}$$

These separable terms of subband energy and kinetic energy will be exploited in next subsections.

3.2.2 The Transport Problem

The original 2D EME in Equation (7) can be rewritten in term of wavefunction as below

$$\left[-\frac{\hbar^2}{2m_{11}}\frac{\partial^2}{\partial x^2}-i\frac{\hbar^2k_y}{2m_{12}}\frac{\partial}{\partial x}+\frac{\hbar^2k_y^2}{2m_{22}}+\overline{H_z+W(x,z)}\right]\Psi\left(-i\frac{\partial}{\partial x},k_y:x,z\right)=E\Psi\left(-i\frac{\partial}{\partial x},k_y:x,z\right) \tag{11}$$

After applying the confinement eigenvalues from Equation (8), Equation (11) becomes

$$\sum_m \phi_n^*(x,z)\left[H_{trans} + \epsilon_m\left(x + \frac{m_{33}}{m_{31}}z\right)\right]\phi_m(x,k_y) = E\sum_m \phi_n^*(x,z)\,\phi_m(x,z)\chi_m(x,k_y) \tag{12}$$

with the transport Hamiltonian is given by

$$H_{trans} = -\frac{\hbar^2}{2m_1'}\frac{\partial^2}{\partial x^2} - i\frac{\hbar^2 k_y}{m_{12}'}\frac{\partial}{\partial x} + \frac{\hbar^2 k_y^2}{2m_2'} \tag{13}$$

where some new effective masses are formed by regrouping the terms as

$$\frac{1}{m_1'} = \left(\frac{1}{m_{11}} - \frac{m_{33}}{m_{31}^2}\right) \tag{14}$$

$$\frac{1}{m_2'} = \left(\frac{1}{m_{22}} - \frac{m_{33}}{m_{23}^2}\right) \tag{15}$$

$$\frac{1}{m_{12}'} = \left(\frac{1}{m_{12}} - \frac{m_{33}}{m_{23}m_{31}}\right) \tag{16}$$

$$\frac{1}{m_2''} = \left(\frac{1}{m_2'} - \frac{m_1'}{m_{12}'^2}\right) \tag{17}$$

Equation (12) can be simplified by using canonical transformation, orthogonality condition and Taylor series expansion to yield a general full 3D transport coupled-mode-space equation as

$$\begin{aligned}\left[-\frac{\hbar^2}{2m_1'}\frac{\partial^2\psi_n(x)}{\partial x^2} + \epsilon_n(x)\psi_n(x)\right] + \sum_m W_{nm}(x)\psi_m(x) + \frac{\hbar^2}{2m_1'}\sum_m\left\{\psi_m(x)\int dz\left[\phi_m(x,z)\frac{\partial^2\phi_n^*(x,z)}{\partial x^2}\right] + \right.\\ \left. 2\int dz\frac{\partial\phi_n^*(x,z)}{\partial x}\frac{\partial[\phi_m(x,z)\psi_m(x)]}{\partial x}\right\} = \left(E - \frac{\hbar^2 k_y^2}{2m_2''}\right)\psi_n(x)\end{aligned} \tag{18}$$

The summation terms consisting of coupling $W_{nm}(x)$ among the energy subbands, which represents Zener Tunneling caused by the misalignment of ellipsoid axes and device axes as well as varying cross section of the channel. Equation (18) represents the generalized equation for arbitrary case of wafer orientations and any channel materials [22]. In this study, the specific case is Si (100) nanodevices. In Si (100) devices, the summation terms dealing with $W_{nm}(x)$ are absent because device axes are aligned properly with ellipsoid axes. The kinetic energy's cross terms never arise in Si (100) MOSFETs. Moreover, the potential energy's cross terms can be ignored in a channel structure with uniformly unvarying cross section. The DG nano-MOSFET shown in Figure 1 with Table 1 structural parameters satisfied these two criteria.

3.2.3 Ultra-Thin Body (UTB) Transistors

With the following conditions, Equation (18) can be simplified to Equation (19) :-

i. Uniform device cross section which allows transport and confinement potentials to be treated separately.
ii. No Zener Tunneling between subbands due to slow varying channel-directed potential, $V(x)$.

$$-\frac{\hbar^2}{2m_1'}\frac{\partial^2\psi_n(x)}{\partial x^2} + V(x)\psi_n(x) = \left(E - \epsilon_n - \frac{\hbar^2 k_y^2}{2m_2''}\right)\psi_n(x) \tag{19}$$

The above simplification is valid in nanoscale n-MOSFET where body structural dimension is in the regime of nanometer. The transformation technique described here maps each conduction band ellipsoid into a corresponding regular ellipsoid whose principal axes is the same as device coordinate axes. Now, the equivalent effective masses at axes x, y and z are m'_1, m''_2, and m_{33}, respectively.

3.3 Applications to UTB Si-Based (100) Oriented DG Nano-MOSFET

3.3.1 DCS Transformation Matrix for (100) Wafer

In the simulation and fabrication of nanoscale silicon MOSFETs, (100) oriented wafers is the most commonly used. The inversion charge layer is confined along [001] direction which is equivalent to z axis for DCS. Meanwhile, the transport and width directions, which are equivalent to x and y axes, are along [100] and [010], respectively. Therefore, the transformation matrix, $\Re_{C\leftarrow D}$ is an identity matrix given by

$$\Re_{C\leftarrow D}^{(001)} = \begin{bmatrix} 1 & 0 & 0 \\ 0 & 1 & 0 \\ 0 & 0 & 1 \end{bmatrix} \tag{20}$$

3.3.2 The ECS Transformation Matrix for Δ-Valley

Since Si is indirect band-gap semiconductor, it has sixfold degenerate Δ-valleys which are populated by conduction band electrons (see to Figure 2) and so Λ-valleys can be ignored for transport analysis. On the contrary, Λ-valleys are more populated with conduction band electrons in Ge. Since only 1 subband of the unprimed valleys is considered in this study, the conduction band constant energy ellipsoid $\Re_{E\leftarrow C}$ transformation matrix becomes

$$\Re_{E\leftarrow C}^{\Delta_1} = \begin{bmatrix} 1 & 0 & 0 \\ 0 & 1 & 0 \\ 0 & 0 & 1 \end{bmatrix} \tag{21}$$

Then, the overall rotation matrix $\Re_{E\leftarrow D}$ can be evaluated by Equation (3). After that, the effective mass tensor, $[M_D^{-1}]$ in DCS is determined from Equation (4) [23].

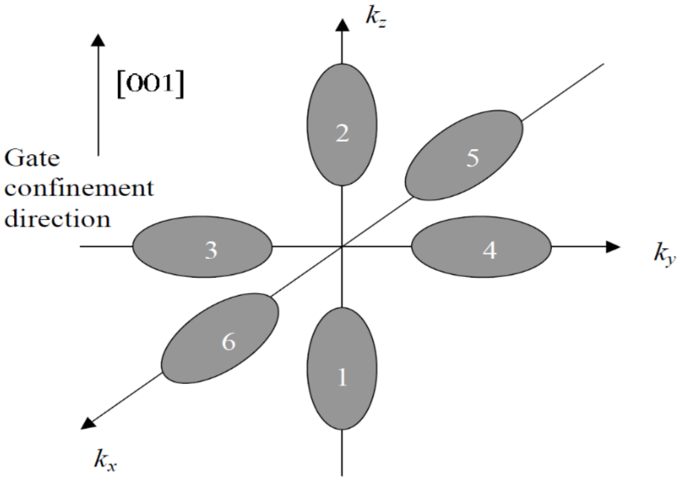

Fig. 2 *Six equivalent conduction band ellipsoids. The unprimed subbands are due to gate confinement of ellipsoids 1 and 2 with a heavier longitudinal effective mass. In addition, the primed subbands are caused by ellipsoids 3 to 6 with a lighter transverse effective mass*

3.3.3 Electron Transport Models in DG Nano-MOSFET

Two drain current models are used to evaluate the compatibility of the theoretical models and simulation result. The first model is based on electrostatics and the drain current per micro width is expressed as

$$\frac{I_D}{W} = BC_{ox}v_T(V_{GS}-V_T)\left[\frac{1-\dfrac{\mathcal{F}_{1/2}\left(\eta_{F1}-\dfrac{qV_D}{k_BT}\right)}{\mathcal{F}_{1/2}(\eta_{F1})}}{1+\dfrac{\mathcal{F}_0\left(\eta_{F1}-\dfrac{qV_D}{k_BT}\right)}{\mathcal{F}_0(\eta_{F1})}}\right] \tag{22}$$

Refer to author paper [24] for detailed explanation of Equation (22). The second model is based on flux-theory approach and the drain current per micron width is given by

$$\frac{I_d^{BAL}}{W} = q\left({F_s}^{+} - {F_d}^{-}\right) \tag{23}$$

Refer to author paper [25] and reference [26] for detailed explanation of Equation (23).

4. Results and Discussion

In the previous sections, a generalized effective mass equation with quantum mechanical formalism has been introduced in the context of cubic semiconductor n-type nano-MOSFET with arbitrary wafer orientations and any channel materials. In such nanotransistors, the conduction band energy ellipsoid principal axes do not align properly with device coordinate axes. Thus, the computational solution of the EME is tedious or non-trivial. This short coming is overcome by applying the technique of transforming the principal axes of the conduction band ellipsoid so that they align with the device axes and thereby enable device scientist to use any device simulator with EME model to investigate n-MOSFET with arbitrary wafer orientations and various channel materials [27].

In this study, Si-based wafer with orientation (100) is chosen since this is the most common wafer type for fabricating CMOS ICs, such as logic gates [28]. Here are the steps involve in this transformation technique for S-based (100) wafer:

i. The appropriate $\Re_{C\leftarrow D}$ is stated in Equation (20).

ii. The suitable $\Re_{E\leftarrow C}$ is stated in Equation (21). Since Δ-valleys has lower energy state than Λ-valleys and therefore populated with electrons. Also, it is sufficient to consider only 1 subband energy because splitting of energy levels due to quantization is large compared to thermal voltage at room temperature, that is simulation temperature.

iii. Next, $\Re_{E\leftarrow D}$ is evaluated by using Equation (3) as

$$\Re_{E\leftarrow D} = \begin{bmatrix} 1 & 0 & 0 \\ 0 & 1 & 0 \\ 0 & 0 & 1 \end{bmatrix} \tag{24}$$

iv. After that, effective mass tensor, $[M_D^{-1}]$ in DCS is determined using Equation (4) as

$$[M_D^{-1}] = \begin{bmatrix} 1.120 \times 10^{30} & 0 & 0 \\ 0 & 5.778 \times 10^{30} & 0 \\ 0 & 0 & 5.778 \times 10^{30} \end{bmatrix} \tag{25}$$

v. Then, from Equation (14), transport effective mass, m_X $(= m_1')$, is obtained as 8.927×10^{-31} kg. Also, from Equation (17), width effective mass, m_Y $(= m_2'')$, is obtained as 1.731×10^{-31} kg. Finally, confinement effective mass, m_Z $(= m_{33})$ is directly obtained from the effective mass tensor, $[M_D^{-1}]$ as 1.731×10^{-31} kg.

In Si (100) wafer, the principal axes of conduction band is properly aligned with device axes. The shape of the conduction band energy contours are ellipses in shape and the transformed ellipsoid volume remains the same as the original one. This conservation of ellipsoidal volume causes the quantum mechanical simulation of the DG nano-MOSFET using m_X, m_Y and m_Z to produce identical result with the simulation outcome from treating the nondiagonal effective mass tensor, $[M_D^{-1}]$. This statement can be verified by benchmarking I-V simulation output with theoretical drain current models as will be discussed next.

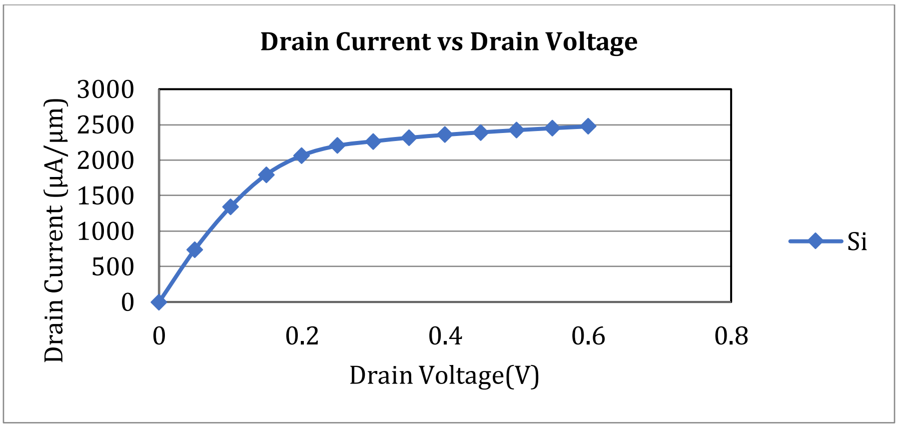

Fig. 3 *Drain current versus drain-to-source voltage*

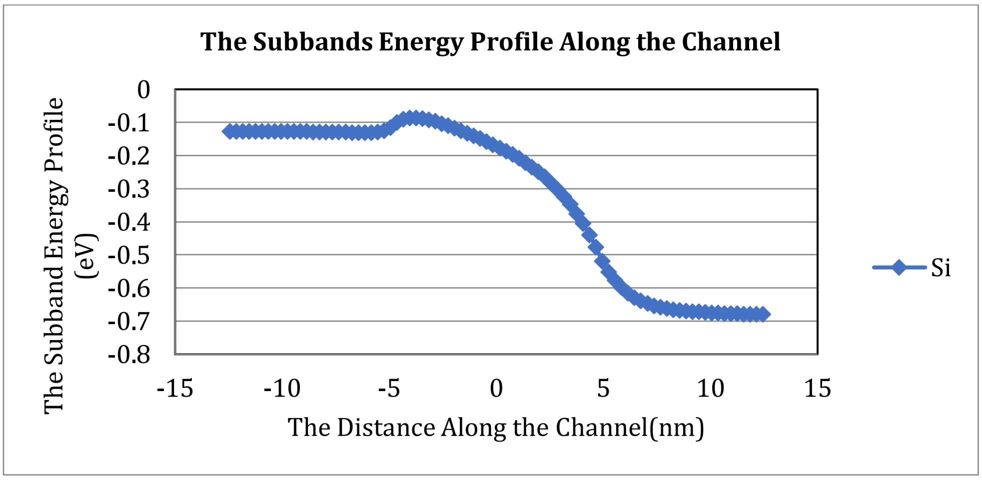

Fig. 4 *Subband energy profile along the Si channel*

Figure 3 and Figure 4 show the I-V curve and the subband energy profile along the Si channel with constant cross section, respectively [29, 30] from the nanoMOS output simulation plots. From Figure 3, the simulated I_{on} is 2.500x10³ μA/μm. The first model in Equation (22), which includes scatterings, is quantum mechanical in nature and produces a theoretical value of 2.182x10³ μA/μm. The accuracy of this model is 87.28% because of the presence of scatterings. The second model in Equation (23) is based on flux-theory approach producing a theoretical value of 2.548x10³ μA/μm and an accuracy of almost 100% because the electron transport is ballistic in nature. Therefore, this second model is useful in depicting high speed logic circuits [31]. These key findings are tabulated in Table 3.

Table 3 *Key findings of on-state current for comparison between simulation model and theoretical models*

Transport Model	Simulation Model	Theoretical Model Based on Electrostatics	Theoretical Model Based on Flux Theory Approach
Current Value (μA/μm)	2500	2182	2548
Percentage of Accuracy	Benchmarked Value	87.28%	≈100%

The simulation result of this paper is benchmarked against the practical measurement data of an UTB InGaAs-OI (Indium Gallium Arsenide-on-insulator) nMOSFET structure configuration as cited from the research work in reference [32]. The new channel material and wafer used by the authors are InGaAs and Ge wafer, respectively. Table 4 summarizes these comparisons. From this table, it is noticed that both MOSFET structures have a high on-to-off current ratio, verifying that excellent gate control can be found is both devices and thus alleviating short channel effects. The transformation technique discussed in this paper can be applied to the investigation of InGaAs-OI nMOSFET by simulation.

Table 4 *Benchmarking between Si-based double-gate nano-MOSFET and InGaAs-OI MOSFET*

Device Struicture	Double-Gate (DG) nMOSFET	On-Insulator (OI) nMOSFET
Channel Material	Silicon (Si) (Elementary Subastance)	Indium Gallium Arsenide (InGaAs) (III-V Compound)
Oxide Insulator	Silicon Dioxide (SiO_2)	Aluminium Oxide (Al_2O_3)
Channel Length	10 nm	100 µm
Channel Width	1 µm	20 µm
Drain Voltage	0.60 V	1.00 V
On-state Current	2500 µA/µm	3.38 µA/µm
Off-state Leakage Current	$5.3x10^{-2}$ µA/µm	$1.0x10^{-6}$ µA/µm
On-to-Off Current Ratio	$5x10^4$	$3x10^6$

5. Conclusion

From the discussion section, it is evident that ultra-thin body n-type DG nano-MOSFET with arbitrary wafer orientations and any channel materials can be investigated using any device simulator equipped with effective mass equation model provided that the arbitrarily oriented conduction band energy ellipsoids principal axes are mapped into regular ellipsoids with the same volume along the device axes. This method can generate accurate electrical characteristics, such as I-V curve and subband energy profile, which helps device scientists to explore the electron transport properties of nano-MOSFET with any channel materials and arbitrary wafer orientations. Device engineers can leverage simulations of novel channel materials and arbitrary wafer orientation of nanoscale MOSFETs to perform optimization on the device electrical performance, predict reliability issues and explore new process technologies. All these efforts can ultimately lead to faster, smaller and more efficient nanoscale transistors.

Acknowledgement

A special thanks to students at Faculty of Information and Communication Technology, Universiti Tunku Abdul Rahman for their enthusiastic interests in this research area.

Conflict of Interest

Authors declare that there is no conflict of interests regarding the publication of the paper.

Author Contribution

The authors confirm contribution to the paper as follows: ***study conception and design:*** *Ooi Chek Yee;* ***data collection:*** *Ooi Chek Yee;* ***analysis and interpretation of results:*** *Ooi Chek Yee;* ***draft manuscript preparation:*** *Ooi Chek Yee, Wong Pei Voon. All authors reviewed the results and approved the final version of the manuscript.*

References

[1] Simone Palazzo, Annunziata Sanseverino, Giovanni Canale Parola, Emanuele Martano, Francesco Velardi and Giovanni Busatto (2024). A simple thermal model for junction and hot spot temperature estimation of 650 V GaN HEMT during short circuit, *Electronics, 13*, 2189. https://doi.org/10.3390/electronics13112189

[2] Do-Kywn Kim, Saungeun Park, Jae-Phil Shim and Seung Heon Shin (2023). Performance of flexible $In_{0.7}Ga_{0.3}As$ MOSFETs by utilizing liquid polyimide (LPI) transfer with effective mobility of 3,667 cm^2/V-s, *Solid State Electronics, Elsevier*, 206(2023) 108672. https://doi.org/10.1016/j.sse.2023.108672

[3] Peng Li, Jialin Liu, Shikai Sun, Wenhao Yang, Yuyin Sun and Yuming Zhang (2024). A voltage equalization strategy for series-connected SiC MOSFET applications, *Electronics*, 13, 3766. https://doi.org/10.3390/electronics13183766

[4] Christopher A. Grome and Wei Ji (2024). A brief review of single-event burnout failure mechanisms and design tolerances of silicon carbide power MOSFETs, *Electronics*, 13, 1414. https://doi.org/10.3390/electronics13081414

[5] Ines Hausler, Rostislav Repa, Adnan Hammud, Oliver Skibitzki and Fariba Hatami (2024). Investigation of defect formation in monolithic integrated GaP islands on Si nanotip wafers, *Electronics*, 13, 2945. https://doi.org/10.3390/electronics13152945

[6] Bao Rong Chang, Hsiu-Fen Tsai and Yi-Ru Wu (2024). Detection and prediction of probe mark damage in wafer testing, *Electronics*,13, 4075. https://doi.org/10.3390/electronics13204075

[7] Cristina Medina-Bailon, Tapas Dutta, Ali Rezaei, Daniel Nagy, Fikru Adamu-Lema, Vihar P. Georgiev and Asen Asenov (2021). Simulation and modeling of novel electronic device architectures with NESS (Nano-electronic simulation software): a modular nano TCAD simulation framework, *Micromachines*, 12, 2021, 680. https://doi.org/10.3390/mi12060680

[8] Zlatan Stanojevic, Chen-Ming Tsai, Georg Strof, Ferdinand Mitterbauer, Oskar Baumgartner, Christian Kernstock and Markus Karner (2021). Nano device simulator – a practical subband-BTE solver for path-finding and DTCO, *IEEE Transactions on Electron Devices*, 68(11), 5400-5406.

[9] Izwanizam Yahaya, A. H. Afifah Maheran, F. Salehuddin and K. E. Kaharudin (2022). Design and electrical simulation of 22 nm MOSFET with graphene bilayer channel using double high-k metal gate, *International Journal of Nanoelectronics and Materials*, 15(2), 70-90.

[10] Jinsik Kim and Inwhee Joe (2024). Chip-level defect analysis with virtual bad wafers based on huge big data handling for semiconductor production, *Electronics*, 13, 2205. https://doi.org/10.3390/electronics13112205

[11] Ooi Chek Yee (2019). Device-circuit level simulation study of three inputs complex logic gate designed using nano-MOSFETs, *Applications of Modelling and Simulation, Malaysia Simulation Society,* UTM, Volume 3, Issue 1, pp 1-10.

[12] Ooi Chek Yee and Lim Soo King (2017). Nano-MOSFETs implementation of different logic families of two inputs NAND gate transistor level circuits: a simulation study, *Jurnal Teknologi,* UTM, Volume 79, Issue 7, pp 41-49.

[13] Ooi Chek Yee and Lim Soo King (2016). Simulation study on different logic families of NOT gate transistor level circuits implemented using nano-MOSFETs, *Journal of Telecommunication, Electronic and Computer Engineering*, UTeM, Malaysia, Volume 8, Issue 5, pp 61-67.

[14] Ooi Chek Yee, Mok Kai Ming and Wong Pei Voon (2021). Device and circuit level simulation study of NOR gate logic families designed using nano-MOSFETs, *PLATFORM – A Journal of Science and Technology*, *UTP Press*, Volume 4, Number 1, pp 73-84.

[15] Ooi Chek Yee and Lim Soo King (2016). A comparative study of quantum gates and classical logic gates implemented using solid-state double-gate nano-MOSFETs, *International Journal of Nanoelectronics and Materials*, 9, 123-132.

[16] Md. Rokib Hasan (2017). Influence of device performance of sub-10 nm GaN-based DG-MOSFET over conventional Si-based SG-MOSFETs, *Proceedings of the 2017 4th International Conference on Advances in Electrical Engineering*, Dhaka, Bangladesh, 2017, 697-702.

[17] Xufeng Wang (2010). Nanomos 4.0: a tool to explore ultimate Si transistors and beyond. [Master of Science Thesis, Purdue University].

[18] Zhibin Ren (2001). Nanoscale MOSFETs: physics, simulation and design. [Ph.D. Thesis, Purdue University].

[19] Abdolreza Darabi, Mohammad Reza Salehi and Ebrahim Abiri (2023). Single-sided gate-wrap-around CNTFET SRAM cell for utilization in reliable IoT-based platforms, *International Journal of Electronics and Communications, Elsevier,* 163(2023) 154605. https://doi.org/10.1016/j.aeue.2023.154605

[20] Tabassum Khurshid and Vikram Singh (2023). Energy efficient design of unbalanced ternary logic gates and arithmetic circuits using CNTFET, *International Journal of Electronics and Communications, Elsevier*, 163(2023) 154601. https://doi.org/10.1016/j.aeue.2023.154601

[21] Anisur Rahman (2005). Exploring new channel materials for nanoscale CMOS devices: a simulation approach. [Ph.D. Thesis, Purdue University].

[22] Anisur Rahman, Gerhard Klimeck, T. B. Boykin and Mark Lundstrom (2004). Bandstructure effects in ballistic nanoscale MOSFETs, *IEDM Technical Digest*, 139-142.

[23] Rahman, A. Ghosh and M. Lundstrom (2003). Assessment of Ge n-MOSFETs by quantum simulation, *IEDM Technical Digest*, 19.4.1-19.4.4.

[24] Ooi Chek Yee and Wong Pei Voon (2021). A flexibility and accuracy comparison study of different current-voltage equations for double-gate nano-MOSFET by simulation and theory, *Applications of Modelling and Simulation, ARQII Publication,* Malaysia, Volume 5, pp 200-206.

[25] Ooi Chek Yee (2023). Benchmarking study of ballistic current transport equations in symmetric double-gate nano-MOSFET by using numerical calculations and simulation, *Applications of Modelling and Simulation, ARQII Publication,* Malaysia, Volume 7, Issue 2023, pp 1-7.

[26] Raphael Clerc and Gerard Ghibaudo (2013). Analytical models and electrical characterization of advanced MOSFETs in the quasi ballistic regime, *International Journal of High Speed Electronics and Systems*, 22(1) 1350002.

[27] N. H. N. M. Nizam, Afifah Maheran A. H., F. Salehuddin, K. E. Kaharudin and Noor Faizah Z. A. (2023). Virtual fabrication of 14 nm gate length n-type double-gate MOSFET, *International Journal of Nanoelectronics and Materials*, Volume 16, 43-51.

[28] N. Aruna Kumari and P. Prithvi (2023). A comprehensive analysis and performance comparison of CombFET and NSFET for CMOS circuit applications, *International Journal of Electronics and Communications, Elsevier,* 158(2023) 154447. https://doi.org/10.1016/j.aeue.2022.154447

[29] Ooi Chek Yee (2015). Simulation study on the electrical performance of equilibrium thin-body double-gate nano-MOSFET, *Jurnal Teknologi,* UTM, Volume 76, Issue 1, pp 87-95.

[30] Ooi Chek Yee (2016). Simulation study of 2D electron density in primed and unprimed subband thin-body double-gate nano-MOSFETof three different thicknesses and two temperature states, *International Journal of Nanoelectronics and Materials*, 9, 67-84.

[31] Ooi Chek Yee (2023). Numerical analysis study of the effects of backscattering coefficient on electrical performance of double-gate nano-MOSFET, *PLATFORM – A Journal of Science and Technology*, *UTP Press*, Volume 6, Number 1, pp 25-32.

[32] Xiaoyu Tang, Yujie Liu, Zhezhe Han and Tao Hua (2024). Carrier mobility enhancement in ultrathin-body InGaAs-on-insulator n-channel metal-oxide-semiconductor field-effect transistors based on dual-gate modulation, *Electronics*, 13, 3893. https://doi.org/10.3390/electronics13193893